

Influence of anisotropy on the electrical conductivity and diffusion coefficient of dry K-feldspar: Implications of the mechanism of conduction

Li-Dong Dai(代立东), Hai-Ying Hu(胡海英), He-Ping Li(李和平), Wen-Qing Sun(孙文清), Jian-Jun Jiang(蒋建军)
Citation: Chin. Phys. B . 2018, 27(2): 028703. **doi:** 10.1088/1674-1056/27/2/028703

Journal homepage: http://cpb.iphy.ac.cn; http://iopscience.iop.org/cpb

What follows is a list of articles you may be interested in

Anisotropic formation mechanism and nanomechanics for the self-assembly process of cross-*β* peptides

Li Deng(邓礼), Yurong Zhao(赵玉荣), Peng Zhou(周鹏), Hai Xu(徐海), Yanting Wang(王延颋)
Chin. Phys. B . 2017, 26(12): 128701. **doi:** 10.1088/1674-1056/26/12/128701

In-situ high pressure X-ray diffraction studies of orthoferrite $SmFeO_3$

Li Na-Na, Li Yan, Li Hui, Tang Rui-Lian, Zhao Yong-Sheng, Han Dan-Dan, Ma Yan-Mei, Cui Qi-Liang, Zhu Pin-Wen, Wang Xin
Chin. Phys. B . 2014, 23(6): 069101. **doi:** 10.1088/1674-1056/23/6/069101

In-situ high-pressure behaviors of double-perovskite Sr_2ZnTeO_6

Han Dan-Dan, Gao Wei, Li Na-Na, Tang Rui-Lian, Li Hui, Ma Yan-Mei, Cui Qi-Liang, Zhu Pin-Wen, Wang Xin
Chin. Phys. B . 2013, 22(5): 059101. **doi:** 10.1088/1674-1056/22/5/059101

First principles calculations of alloying element diffusion coefficients in Ni using the five-frequency model

Wu Qiong, Li Shu-Suo, Ma Yue, Gong Sheng-Kai
Chin. Phys. B . 2012, 21(10): 109102. **doi:** 10.1088/1674-1056/21/10/109102

Influence of anisotropy on the electrical conductivity and diffusion coefficient of dry K-feldspar: Implications of the mechanism of conduction*

Li-Dong Dai(代立东)[1,†], Hai-Ying Hu(胡海英)[1], He-Ping Li(李和平)[1], Wen-Qing Sun(孙文清)[1,2], and Jian-Jun Jiang(蒋建军)[1]

[1] *Key Laboratory of High-temperature and High-pressure Study of the Earth Interior, Institute of Geochemistry, Chinese Academy of Sciences, Guiyang* 550081, *China*

[2] *University of Chinese Academy of Sciences, Beijing* 100049, *China*

(Received 7 October 2017; revised manuscript received 3 November 2017; published online 5 January 2018)

The electrical conductivities of single-crystal K-feldspar along three different crystallographic directions are investigated by the Solartron-1260 Impedance/Gain-phase analyzer at 873 K–1223 K and 1.0 GPa–3.0 GPa in a frequency range of 10^{-1} Hz–10^{6} Hz. The measured electrical conductivity along the $\perp$[001] axis direction decreases with increasing pressure, and the activation energy and activation volume of charge carriers are determined to be 1.04 ± 0.06 eV and 2.51 ± 0.19 cm^3/mole, respectively. The electrical conductivity of K-feldspar is highly anisotropic, and its value along the $\perp$[001] axis is approximately three times higher than that along the $\perp$[100] axis. At 2.0 GPa, the diffusion coefficient of ionic potassium is obtained from the electrical conductivity data using the Nernst–Einstein equation. The measured electrical conductivity and calculated diffusion coefficient of potassium suggest that the main conduction mechanism is of ionic conduction, therefore the dominant charge carrier is transferred between normal lattice potassium positions and adjacent interstitial sites along the thermally activated electric field.

Keywords: electrical conductivity and diffusion coefficient, K-feldspar, anisotropy, conduction mechanism

PACS: 87.15.Pc, 91.25.St, 91.60.Dc, 91.60.Gf **DOI:** 10.1088/1674-1056/27/2/028703

1. Introduction

The explanation of geomagnetic deep sounding and magnetotelluric (MT) data from the deep interiors of earth's and other planets' deep interior relies on the known electrical properties of minerals and rocks established in the laboratory at the relevant temperatures and high pressures.[1–7] The MT field surveys have found zones of anomalously high conductivity ($\sim 10^{-2}$ S/m–10^{-1} S/m) and highly anisotropic electrical conductivity in many parts of the lithosphere and asthenosphere.[8–13] The *in-situ* measurements of laboratory-based electrical conductivities of minerals along different crystallographic axes can help us to explain the degree of anisotropy from MT results, which have been observed to be as high as 100 in the mantle and perhaps 1000 in the lower crust.

Feldspar is a representative tectosilicate mineral characterized by a fundamental formula of MT_4O_8 (M denotes Na, Ca, K or Ba; T refers to Si or Al), and is the most abundant rock-forming alumosilicate mineral that contains 60% of the earth's crust; it can be found widespread and commonly in various igneous, metamorphic, and some sedimentary rocks. In general, alkali (K^+, Na^+) or alkaline-earth (Ca^{2+}, Ba^{2+}) cations with large ionic radii occupy the M-sites in the feldspar crystal structure. The T-sites are occupied by a three-dimensional (3D) framework of different charges of tetrahedral Al^{3+} and Si^{4+} ions, which are widely used in the glass, ceramics, and cement industries. The composition and structural stability of feldspar make it an important component of the earth's crust; its electrical properties at high temperatures and high pressures, combined with those of other typical rock-forming minerals in the deep crust (e.g., quartz, amphibole, clinopyroxene, orthopyroxene and mica) are crucial to establishing the conductivity–depth profile of the earth's interior.[14–19]

The electrical conductivities of natural and synthetic alkali feldspar (both K-feldspar ($KAlSi_3O_8$) and albite ($NaAlSi_3O_8$), and their solid solution), anorthite ($CaAl_2Si_2O_8$), and plagioclase have been extensively studied at high temperatures and high pressures.[20–34] It is important to know the electrical conductivity of K-feldspar, a crucial end member of feldspar, for explaining the conduction mechanism of K-feldspar-bearing rock deep in the earth's crust. However, the several studies that have previously investigated this are limited in scope. Maury studies[23] reported the electrical conductivities of a series of polycrystalline feldspars

*Project supported by the Strategic Priority Research Program (B) of the Chinese Academy of Sciences (CAS) (Grant No. XDB 18010401), the Key Research Program of Frontier Sciences of CAS (Grant No. QYZDB-SSW-DQC009), the "135" Program of the Institute of Geochemistry of CAS, the Hundred-Talent Program of CAS, and the National Natural Science Foundation of China (Grant Nos. 41474078, 41774099, and 41772042).

†Corresponding author. E-mail: dailidong@vip.gyig.ac.cn

© 2018 Chinese Physical Society and IOP Publishing Ltd

at 673 K–1173 K and atmospheric pressure. Guseinov and Gargatsev[26] measured the electrical conductivities of natural pure microcline single-crystal feldspar and the maximum microcline single-crystal of feldspar with a minor albite phase at 373 K–1273 K and atmospheric pressure. Hu *et al.*[30] measured the electrical conductivities of hot-pressed synthetic polycrystalline dry K-feldspar aggregate at 1.0 GPa–3.0 GPa and 873 K–1173 K by using a multi-anvil press, and from the Nernst–Einstein equation they also calculated its diffusion coefficient. More recently, El Maanaoui *et al.*[34] investigated the anisotropic electrical conductivities of natural alkali feldspar from the German Eifel region with two distinct chemical compositions characterized by potassium to total-alkali cation ratios ($X_K = x_K/(x_K + x_{Na} + x_{Rb} + x_{Ba})$) of 0.71 and 0.83 at 573 K–1173 K and atmospheric pressure; they found a weak dependence of electrical conductivity on chemical composition and an obvious anisotropy between conductivity in the $\perp$[010] and $\perp$[001] directions. However, despite K-feldspar importance in the feldspar group, the anisotropy of its electrical conductivity at high temperature and high pressure has not been fully reported previously.

The present study reports the use of impedance spectroscopy to determine the electrical conductivities of single-crystal K-feldspar along three different crystallographic directions at frequencies of 0.1 Hz to 1 MHz. A series of characteristic parameters including the pre-exponential factor, activation energy, and activation volume are acquired. The single-crystal K-feldspar shows a large anisotropic electrical conductivity, and the results are compared with those of previous studies. At 2.0 GPa, the diffusion coefficient of ionic potassium is calculated by using the electrical conductivity data from the Nernst–Einstein equation. We also discuss in detail the conduction mechanism of the K-feldspar single crystal at high temperature (T) and pressure (P).

2. Experimental procedures

2.1. Sample preparation

The natural K-feldspar megacryst in the present study was available from Pakistan. The surface of each sample was fresh, non-fractured, non-oxidized and purely gem-class single-crystal K-feldspar without any evidence of twinning, exsolution, alteration, secondary phase precipitation, structural flaws, or heterogeneity. Chemical compositions (see Table 1) were determined by electron microscopy analyses at the State Key Laboratory of Ore Deposit Geochemistry, Institute of Geochemistry, Chinese Academy of Sciences. Monoclinic K-feldspar was oriented along the [010] crystal plane developed by [010] cleavage, and the other [100] and [001] crystal planes were mutually perpendicular. Samples were drilled along the three corresponding crystallographic orientations, which are termed $\perp$[100] (a-direction), $\perp$[010] (b-direction), and $\perp$[001] (c^*-direction). A detailed crystalline configuration, lattice plane and crystallographic axis for K-feldspar single crystal along three main directions is displayed in Fig. 1. In order to confirm the phase state during electrical conductivity measurement, Raman spectroscopic images were recorded in the process of high-pressure conductivity measurements. Figure 2 shows a typical image of $\perp$[001] crystallographic K-feldspar before and after electrical conductivity measurement, and confirms that there was no phase change during the experiment. In fact, there exists one good consistency of phase stability of K-feldspar with Liu *et al.*'s reported results at similar temperature and pressure conditions[35] The

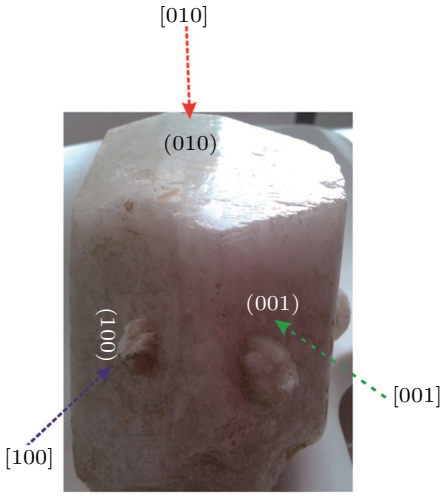


Fig. 1. (color online) Detailed description crystalline configuration, lattice plane and crystallographic axis for K-feldspar single crystal along three main directions.

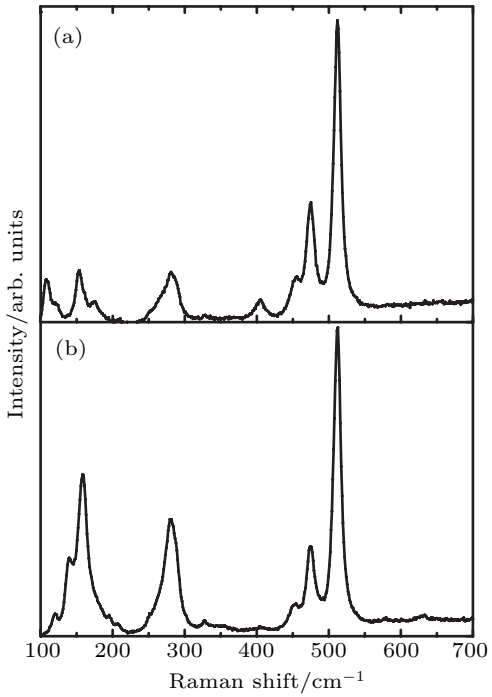


Fig. 2. Raman spectra of the starting material and the recovered sample: (a) the starting material used in this study, (b) the sample recovered from 3 GPa. All peaks are attributed to K-feldspar.

Table 1. Chemical compositions of the starting material of K-feldspar.

Compositions	Content/wt%
SiO_2	65.46 (0.42)
TiO_2	0.03 (0.01)
Cr_2O_3	0.12 (0.03)
Al_2O_3	18.01 (0.08)
FeO	0.05 (0.01)
MnO	0.04 (0.01)
K_2O	16.19 (0.09)
Na_2O	0.06 (0.04)
Total	99.96 (0.56)

K-feldspar samples were cut and polished into cylinders (diameter 6.0 mm, height 6.0 mm) using an ultrasonic drill and diamond saw. They were then cleaned sequentially with deionized distilled water, alcohol, and acetone, and baked for 48 h in a 473-K vacuum drying oven to remove any adsorbed water.

2.2. Sample characterization

Vacuum Fourier transform infrared spectroscopy (FT-IR, Vertex-70V, Hyperion-1000 infrared microscope) at wavenumbers from 350 cm^{-1} to 8000 cm^{-1} was used to determine the water content values of doubly polished samples thinner than 120 μm before and after each conductivity experiment. The IR absorption was measured by using unpolarized radiation from mid-IR light sources, a KBr beam splitter, and an MCT detector with a 100 μm×100 μm aperture. A total of 512 scans were acquired for each sample. Figure 3 shows representative infrared spectra acquired in the ⊥[001] crystallographic direction of K-feldspar before and after electrical conductivity measurements. The Paterson calibration was used to determine the water content from the FT-IR absorption with the equation:[36]

$$C_{OH} = \frac{B_i}{150\xi} \int \frac{K(v)}{(3780 - v)} dv, \quad (1)$$

where C_{OH} is the molar concentration of hydroxyl (ppm wt H_2O or H/10^6 Si), B_i is the density factor (3.19×10^4 cm

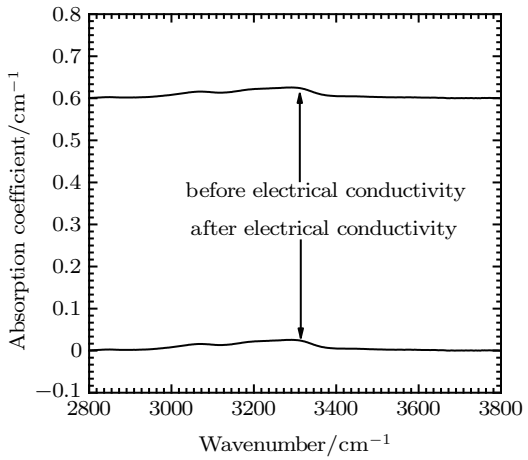


Fig. 3. Representative unpolarized FT-IR spectra of ⊥[001] crystallographic K-feldspar before and after electrical conductivity measurements.

H/10^6 Si), ξ is the orientation factor (1/2), and $K(v)$ is the absorption coefficient in unit cm^{-1} at wavenumber v in unit cm^{-1}. The integration was carried out from 2800 cm^{-1} to 3750 cm^{-1}.

The water content values of K-feldspar before and after conductivity measurements were less than ∼ 6 H/10^6 Si and ∼ 9 H/10^6 Si, respectively, indicating "dry" feldspar. If a modified form of the Beer–Lambert law was chosen to calibrate the water content of K-feldspar, there is a 1 H/10^6–2 H/10^6 Si discrepancy in the obtained water content results.[37] The water content value varied by less than 15% during the electrical conductivity measurements.

2.3. Impedance spectroscopy measurement

In-situ high-pressure electrical conductivity measurements of samples were performed using a YJ-3000t multi-anvil and a Solartron-1260 Impedance/Gain-phase analyzer (Schlumberger) in the Key Laboratory of High-Temperature and High-Pressure Study of the Earth's Interior, Institute of Geochemistry, Chinese Academy of Sciences. Hui *et al.*[38] and Sun *et al.*[39] described in detail the measurement principles and experimental procedures.

The experimental setup for electrical conductivity measurements of feldspar at high pressure is illustrated in Fig. 4. Figure 5 shows the cross-sectional photomicrograph of the high-pressure cell for the recovery assemblage recorded by using plane-polarized reflected light after conductivity measurement. Six symmetric tungsten carbide anvils with a total surface area of 23.4 mm^2 were adopted to generate high-pressure conditions. The melting curves of Cu, Al, Zn, and Pb metals were used in order to precisely calibrate the experimental pressure in the sample cell.[40] Temperature calibration was conducted by virtue of ultrasonic wave velocities of window glass, pyrophyllite, and kimberlite at 1 atm–5.5 GPa (1 atm = 1.01325×10^5 Pa) and 136 °C–1400 °C.[41] Pressure medium of cubic pyrophyllite (32.5 mm×32.5 mm×32.5 mm) was baked at 1073 K for 12 h before electrical conductivity experiments in order to avoid the influence of absorbed water on the electrical conductivity measurements. A Faraday shielding case of 0.05-mm nickel foil, grounded to the Earth, was placed between the pyrophyllite and the Al_2O_3 insulation tube to reduce the temperature gradient inside the sample cell, to minimize current leakage across the pressure medium, and to prevent chemical migration between the sample and the pressure medium. A cylindrical sample (diameter 6.0 mm, height 6.0 mm) was placed in the center of the boron nitride insulation tube and sandwiched between two symmetric, 0.5 mm-thick, metallic nickel electrodes. The experimental temperature in the sample chamber was monitored by a NiCr–NiAl

thermocouple. Measurement errors from the pressure and temperature gradients were less than 0.1 GPa and 10 K, respectively. The uncertainty of the impedance was estimated to be less than 4%, and it was less than 8% obtained from dimensional variations of the samples.

During the experiment, the pressure was raised to the designated value slowly at a rate of 1.0 GPa/h. At a constant pressure, the temperature was then increased gradually at 100 K/h to designated preset values in steps of 50 K. Impedance spectroscopy was measured on a Solartron-1260 Impedance/Gain-phase analyzer with a sinusoidal signal voltage of 1.0 V and a frequency range of 10^{-1} Hz–10^{6} Hz. Four parameters of complex impedance including the real part (Z'), imaginary part (Z''), magnitude ($|Z|$) and phase angle (θ) were obtained from high to low frequency, and satisfied the following equations:

$$\mathrm{tg}\theta = \frac{Z''}{Z'} = \omega RC = \omega\tau_{\mathrm{C}}, \tag{2}$$

$$|Z| = \sqrt{(Z')^2 + (Z'')^2} = \frac{R}{\sqrt{1+(\omega\tau_{\mathrm{C}})^2}}, \tag{3}$$

where ω is the angular frequency (and $\omega = 2\pi f$), f is the frequency, R is the resistance, C is the capacitance, and τ_{C} is the characteristic relaxation time constant. An equivalent circuit made up of the series connection of R_{S}–$\mathrm{CPE_S}$ and R_{E}–$\mathrm{CPE_E}$ was selected to model the impedance semicircles. R_{S} and $\mathrm{CPE_S}$ represent the resistance and the constant phase element of the bulk impedance of the sample, respectively, and R_{E} and $\mathrm{CPE_E}$ represent the resistance and the constant phase element from the polarization effect of the sample–electrode interface, respectively. Measurement errors of electrical conductivity were estimated to be less than 10%.

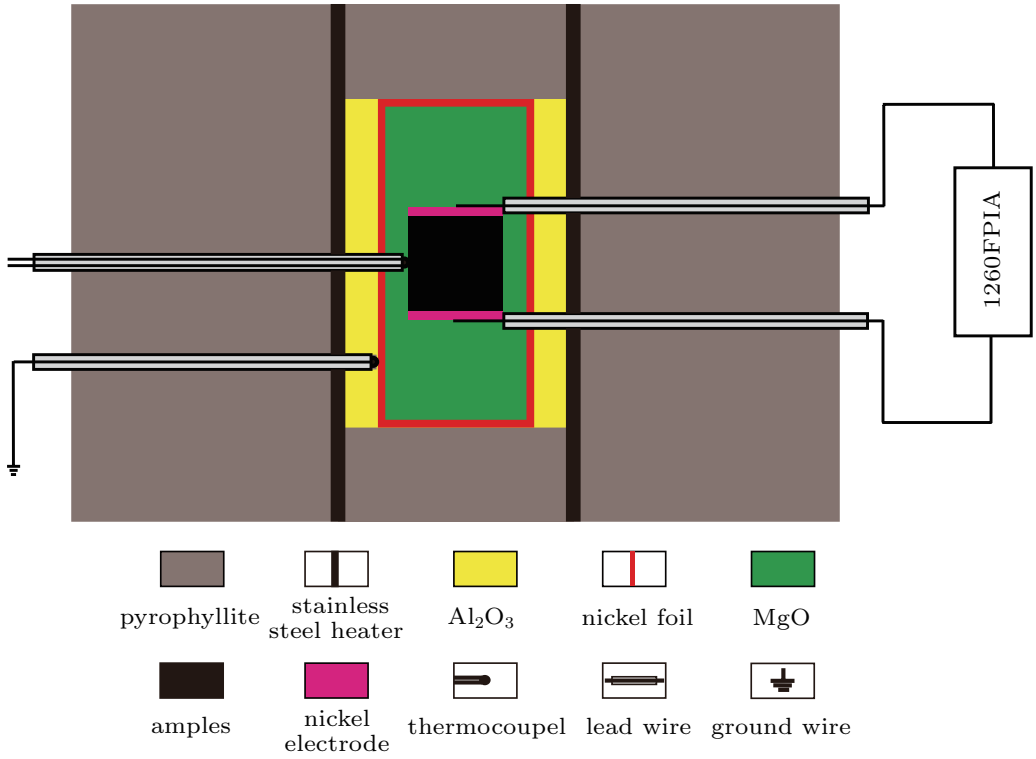


Fig. 4. (color online) Experimental setup for electrical conductivity measurements of feldspar at high pressure.

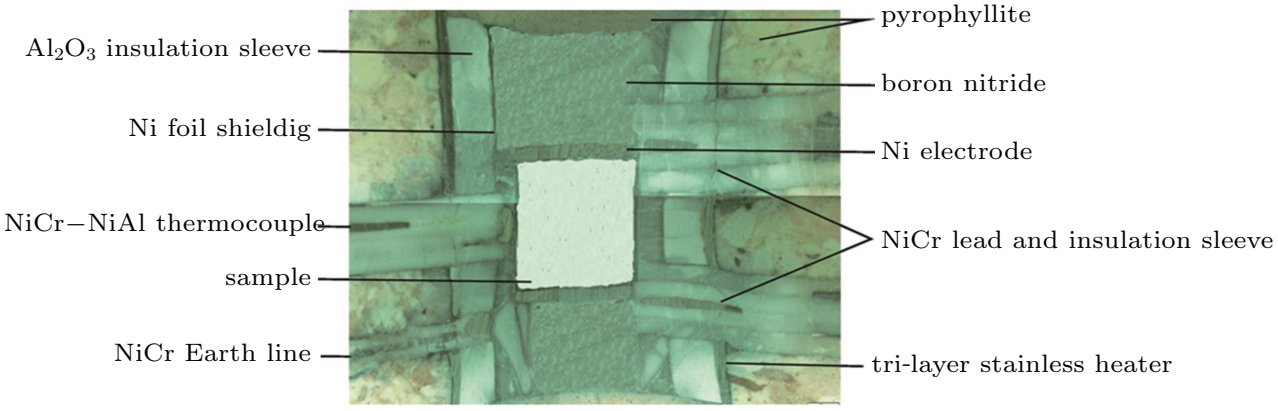


Fig. 5. (color online) Photomicrograph (plane-polarized reflected) taken with light from the recovered sample assembly after conductivity measurement.

3. Results

We measure the electrical conductivity of K-feldspar single crystals along the $\perp[001]$ crystallographic axis under pressures of 1.0 GPa–3.0 GPa and at temperatures of 873 K–1223 K; measurements are also conducted at 2.0 GPa and 873 K–1223 K along the $\perp[100]$ and $\perp[010]$ crystallographic axes. The frequency range of the impedance spectra is 10^{-1} Hz–10^{6} Hz.

Figures 6 and 7 show representative Nyquist and Bode diagrams of the complex spectra for K-feldspar along the $\perp[001]$ crystallographic axis at 2.0 GPa and 873 K–1223 K, which are similar to the results obtained under other conditions. The relations between the real (Z') and imaginary (Z'') parts of the impedance spectra in Fig. 6 clearly show semicircular arcs at relatively high frequencies ($\sim 3\times 10^{2}$ Hz–10^{6} Hz), respectively, representing one transference process for the bulk electrical charge carrier of the sample. The impedance arc shows a small tail at lower frequencies (10^{-1} Hz–$\sim 3\times 10^{2}$ Hz) corresponding to interfacial resistance of the polarization process between the sample and the electrode. The high-frequency ($\sim 10^{6}$ Hz) semicircular arc starts from the origin, and very likely corresponds to an equivalent series combination of R_S–CPE_S and R_E–CPE_E (R_S and CPE_S represent the resistance and the constant phase element of the bulk impedance for the sample, respectively; R_E and CPE_E represent the resistance and the capacitance from the polarization effect of the sample–electrode interface, respectively).[42–45] Figure 7 shows the frequency-dependent real (Z') and imaginary (Z'') parts, magnitude ($|Z|$), and phase angle (φ) of the complex impedance.

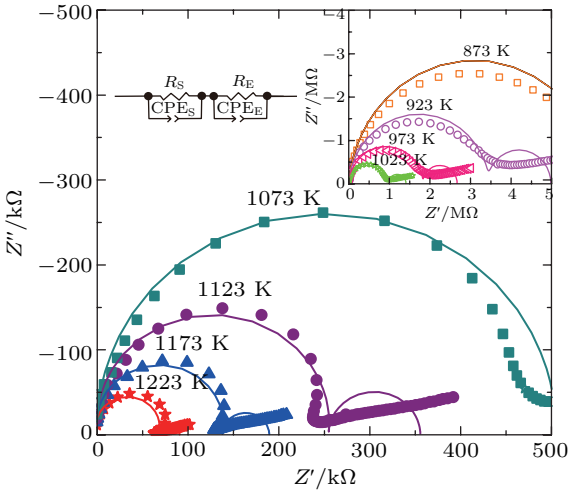


Fig. 6. (color online) Nyquist diagram of impedance spectra for $\perp[001]$ crystallographic K-feldspar at frequencies from 10^{-1} Hz to 10^{6} Hz (from right to left), obtained at 2.0 GPa and 873 K–1223 K. Z' and Z'' are the real and imaginary parts of the complex impedance, respectively. An equivalent circuit composed of the series combination of R_S–CPE_S and R_E–CPE_E is selected to model the complex impedance semicircles.

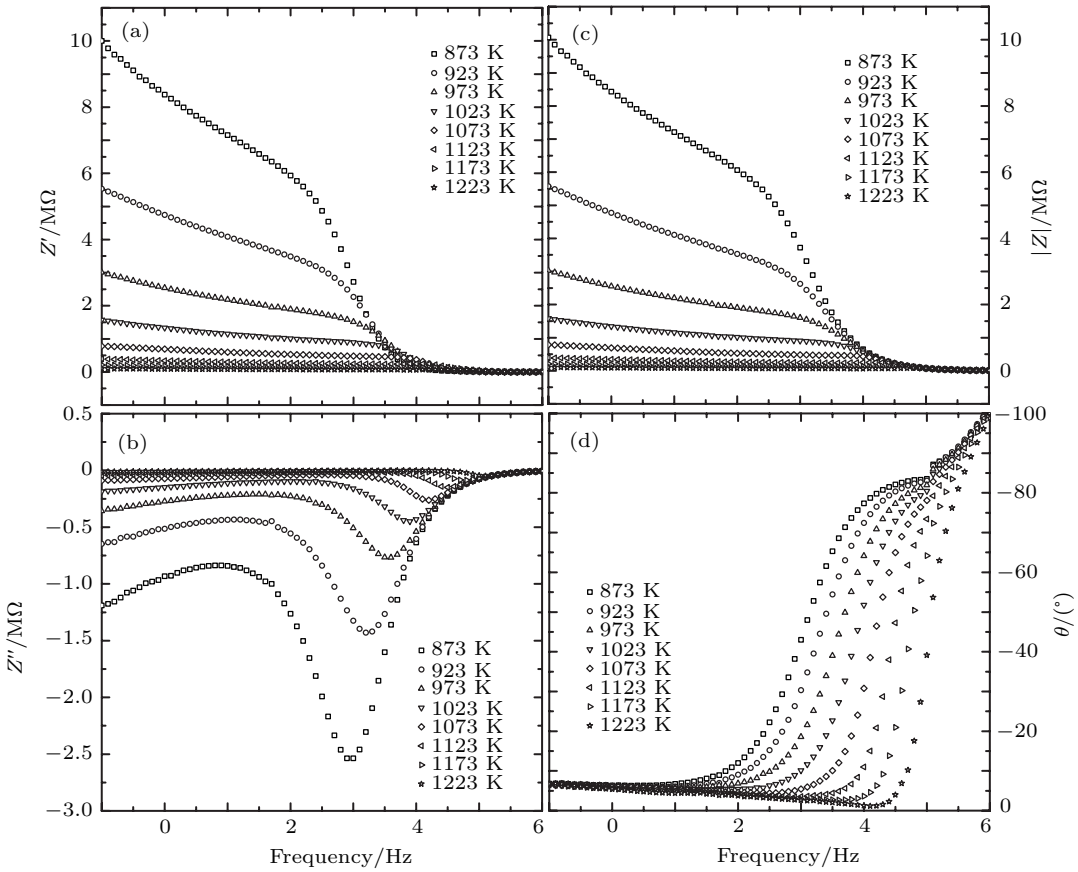


Fig. 7. Bode diagram of the impedance spectra for $\perp[001]$ crystallographic K-feldspar at frequencies from 10^{-1} Hz to 10^{6} Hz (from right to left), obtained at 2.0 GPa and 873 K–1223 K. Panels (a)–(d) respectively show frequency-dependent real (Z') and imaginary (Z'') parts, magnitude ($|Z|$), and phase angle (θ) of the complex impedance.

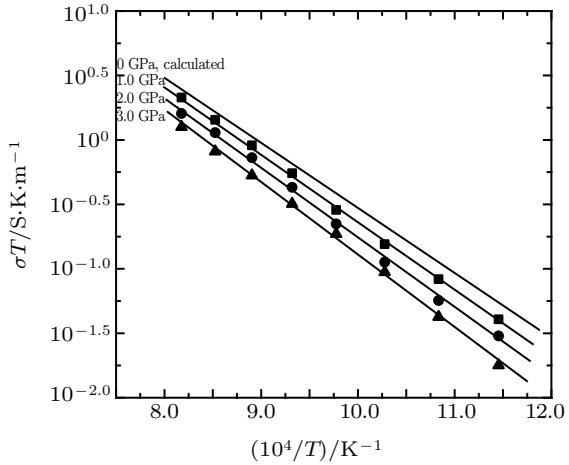


Fig. 8. Influences of pressure on the electrical conductivity of ⊥ [001] crystallographic K-feldspar at 873K–1223 K and different pressures. The calculated electrical conductivity at atmospheric pressure is also shown via the parameters of the Arrhenius relation.

The electrical conductivities of the samples (σ, S/m) are calculated by using the following equation:

$$\sigma = \frac{L/S}{R} = \frac{L}{RS}, \tag{4}$$

where L is the length of sample (in unit m) and S is the cross-sectional area of electrode (m^2). The product of electrical conductivity and temperature satisfy the Arrhenius relation:

$$\sigma T = \sigma_0 \exp(-\Delta H/KT), \tag{5}$$

where σ_0 is the pre-exponential factor (S/m), ΔH is the activation enthalpy (eV), and K is the Boltzmann constant (eV/K). The activation enthalpy (ΔH) is dependent on pressure:

$$\Delta H = \Delta U + P \times \Delta V, \tag{6}$$

where ΔU is the activation energy (eV) and ΔH is the activation volume (cm^3/mole).

Figure 8 shows the influences of pressure on electrical conductivity obtained in the direction perpendicular to the [001] surface of K-feldspar single crystals at 1.0 GPa–3.0 GPa and 873 K–1223 K. Figure 9 shows the electrical conductivities of K-feldspar single crystals along different crystallographic directions at 2.0 GPa and 873K–1223 K. The fitted parameters of the Arrhenius relation are listed in Table 2.

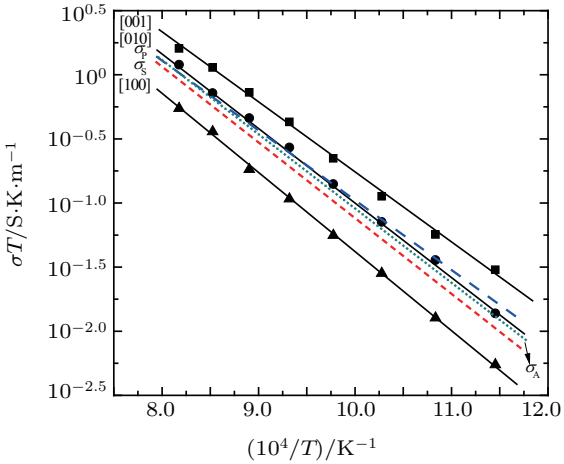


Fig. 9. (color online) Comparison of model average conductivity (series, average and parallel) of polycrystalline feldspar aggregate with electrical conductivity results measured for single crystals at 2.0 GPa.

Table 2. Fitting parameters of Arrhenius relation of electrical conductivity along three crystallographic axes for K-feldspar single crystal at pressures of 1.0 GPa–3.0 GPa. The top five columns represent single crystals in the present study and the bottom three columns refer to the calculated isotropic average values of randomly oriented polycrystalline aggregates. The series, average, and parallel averaging schemes are employed to acquire the electrical conductivities of aggregate sample, i.e., $\sigma_S = \frac{3}{(1/\sigma_{[100]}+1/\sigma_{[010]}+1/\sigma_{[001]})}$, $\sigma_A = \frac{1}{8}[\sigma_S + \sigma_P + \sqrt{(\sigma_S+\sigma_P)^2+32\sigma_S\sigma_P}]$, and $\sigma_P = \frac{(\sigma_{[100]}+\sigma_{[010]}+\sigma_{[001]})}{3}$.

Run No.	Orientation	Pressure/GPa	T/K	σ_0/(S/m)	ΔH/eV	ΔU/eV	ΔV/(cm^3/mole)
DL1602	[001]	1.0	873–1423	47863	1.07±0.01		
DL1608	[001]	2.0	873–1423	48978	1.09±0.04	1.04±0.06	2.51±0.19
DL1611	[001]	3.0	873–1423	52481	1.12±0.01		
DL1613	[010]	2.0	873–1423	72541	1.17±0.02		
DL1620	[100]	2.0	873–1423	56146	1.23±0.03		
	σ_S	2.0	873–1423	68585	1.19±0.02		
	σ_A	2.0	873–1423	57597	1.16±0.03		
	σ_P	2.0	873–1423	49648	1.13±0.01		

4. Discussion

4.1. Influence of pressure and anisotropy

The electrical conductivity of K-feldspar single crystal along the ⊥ [001] crystallographic axis is enhanced by around ∼ 2.1 orders of magnitude as temperature increases from 673 K to 1223 K at constant pressure (Fig. 8). In contrast, it decreases by about ∼ 1.5 times as pressure increases from 1.0 GPa to 3.0 GPa at constant temperature; accordingly, the activation enthalpy slightly increases from 1.07 eV to 1.12 eV, and the pre-exponential factor almost remains a constant value of $10^{4.7}$ S/m (Table 2), which indicates that the ionic mobility of the charge carriers decreases as the feldspar framework is gradually compressed. This suggests a narrower pathway for interstitial charge carriers with increasing pressure, which results in a relatively high energy required for carriers to go across the energy barrier, and thus increasing activation en-

thalpy and reducing the electrical conductivity. The negative pressure dependence of electrical conductivity observed here is consistent with those of tectosilicate sintered polycrystalline aggregates such as albite, K-feldspar, alkali feldspar solid solution, and anorthite reported by Hu *et al.*[28–31] From Eq. (5) and Table 2, we can derive the activation enthalpy and activation volume, under the T and P conditions considered here, to be 1.04 ± 0.06 eV and 2.51 ± 0.19 cm^3/mole, respectively. The electrical conductivity of K-feldspar along the ⊥[001] crystallographic axis at atmospheric pressure can also be calculated using the Arrhenius parameters.

Figure 9 shows the relationship between the logarithmic electrical conductivity along different crystallographic axis directions versus temperature together with results for polycrystalline aggregates obtained by three averaging schemes at 2.0 GPa. The electrical conductivities of K-feldspar in different directions are ranked in the increasing order of ⊥[100], ⊥[010], and ⊥[001], whereas the activation enthalpy in each direction decreases in the same order from 1.23 eV to 1.09 eV (Table 2). The results are highly anisotropic, with the electrical conductivity of K-feldspar in the ⊥[001] direction being approximately ∼ three times higher than that in the ⊥[100] direction. Combining the anisotropic electrical conductivity results for K-feldspar single crystals with a variety of spatial averaging schemes for mixtures of the three phases gives isotropic average values for randomly oriented polycrystalline aggregates. We consider three representative averaging schemes here that give series (σ_S), parallel (σ_P), and average (σ_A) electrical conductivity:

$$\sigma_S = \frac{3}{(1/\sigma_{[100]} + 1/\sigma_{[010]} + 1/\sigma_{[001]})}, \tag{7}$$

$$\sigma_P = \frac{(\sigma_{[100]} + \sigma_{[010]} + \sigma_{[001]})}{3}, \tag{8}$$

$$\sigma_A = \frac{1}{8}[\sigma_S + \sigma_P + \sqrt{(\sigma_S + \sigma_P)^2 + 32\sigma_S\sigma_P}]. \tag{9}$$

These three isotropic average schemes transform the conductivity results along the three crystallographic axes into isotropic conductivity values for randomly oriented polycrystalline K-feldspar aggregates. The results from the series and parallel averaging represent respectively the minimum and maximum average conductivity. However, the present work shows that the magnitude of the anisotropic electrical conductivity of K-feldspar remains approximately constant across the whole temperature range (673 K–1223 K).

4.2. Comparison among previous results and conduction mechanism

Figure 10 shows the comparisons of our current results for the influence of anisotropy on the electrical conductivity of K-feldspar with those from previous experimental studies.[22,23,26,30,34] El Maanaoui *et al.*[34] used electrochemical impedance spectroscopy to investigate the electrical conductivities of single-crystal alkali feldspar in the ⊥[010] and ⊥[001] orientations at 573 K–1173 K and atmospheric pressure; the samples were of two different chemical compositions ($K_{0.71}Na_{0.26}AlSi_3O_8$ and $K_{0.83}Na_{0.15}AlSi_3O_8$), and originated from two different locations — Volkesfeld (VF) and Rockeskyller (RK) sanidine in Eifel, Germany. The electrical conductivity in the c^*-direction (perpendicular to the [001] plane) was distinctly higher than that in the b-direction (perpendicular to the [010] plane), demonstrating obvious anisotropy between the ⊥[010] and ⊥[001] directions of each sample; conductivity also weakly decreased as the potassium site fraction (C_K) increased from 0.71 to 0.83. Hu *et al.*[30] used AC impedance spectroscopy to measure the electrical conductivity of hot-pressed sintered polycrystalline K-feldspar aggregates at 1.0 GPa–3.0 GPa and 873 K–1173 K, and reported a weak negative pressure dependence and a positive activation volume of 1.46 cm^3/mole. Also it is obvious that there is available excellent agreement in the electrical conductivity between polycrystalline K-feldspar aggregates by Hu *et al.*[30] and our present K-feldspar single crystals. Figure 10 shows that the current highly anisotropic conductivity results appear to be consistent with those recently reported for alkali feldspar at atmospheric pressure.[34] The activation enthalpy results obtained here of 1.07 eV–1.23 eV are also very close to the recent values of 0.99 eV–1.02 eV for polycrystalline K-feldspar aggregates reported by Hu *et al.*,[30] 1.05 eV–1.08 eV for single-crystal alkali feldspar reported by Wang *et al.*[33] and 1.04 eV–1.08 eV for single-crystal alkali feldspar reported by El Maanaoui *et al.*,[34] respectively, and also the 0.99 eV migration energy theoretically calculated for K-feldspar by Jones *et al.*[46]

Figure 10 also shows some obvious discrepancies between previous studies and the present work,[22,23,26] which appear mainly to be due to differences in measurement method and in the sample chemical composition. Karato and Dai[47] noted that the possibility of discrepancies is due to systematic errors in the calculations of the electrical conductivity of alkali feldspar by using the direct current (DC) and single-frequency alternating current (AC) techniques of some previous studies.[22,23,26] These previous results for single-crystal feldspar were measured at ambient pressure and high temperature using various chemical compositions: $Or_{61}Ab_{34}An_5$ in Mizutani and Kanamori's work,[22] $Or_{84}Ab_{16}$ in Maury's work,[23] and the microcline–orthoclase phase transition (with a minor albite content) at 1093 K in Guseinov and Gargatsev's work.[26] Like the results for fayalite–forsterite olivine (Fe_2SiO_4–Mg_2SiO_4),[48,49] pyrope–almandine garnet ($Fe_3Al_2Si_3O_{12}$–$Mg_3Al_2Si_3O_{12}$),[50,51] and alkali feldspar and its solid solutions with various percentages

of potassium and sodium ions ($NaAlSi_3O_8$–$KAlSi_3O_8$),[29,34] the chemical composition can also be considered to be a crucial factor influencing the electrical conductivity of feldspar and at least partly responsible for the differences between the previous results and ours.

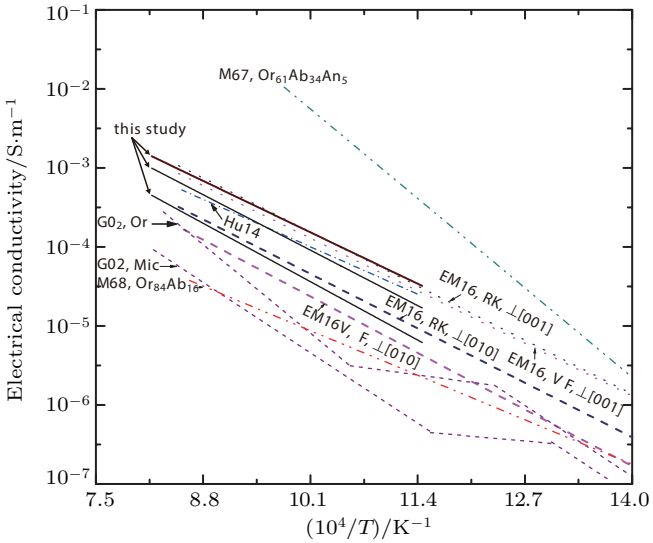


Fig. 10. (color online) Anisotropic electrical conductivities of dry K-feldspar single crystal at 2.0 GPa in the present study compared with previous results. The lines are labeled as follows: black solid lines represent the results of this work; dark blue dashed and dotted lines represent electrical conductivities of the ⊥ [010] and ⊥ [001] orientations of RK alkali feldspar with its chemical composition ($K_{0.71}Na_{0.26}AlSi_3O_8$) from El Maanaoui *et al.*;[34] pink dashed and dotted lines represent electrical conductivities of the ⊥ [010] and ⊥ [001] orientations of VF alkali feldspar with its chemical composition ($K_{0.83}Na_{0.15}AlSi_3O_8$) at atmospheric pressure from El Maanaoui *et al.*;[34] blue short dashed line represents the electrical conductivity of hot-pressed sintered polycrystalline K-feldspar aggregates at 2.0 GPa from Hu *et al.*;[30] two purple dashed lines represent electrical conductivities of the microcline–orthoclase phase transition (with a minor albite content) at room pressure from Guseinov and Gargatsev;[26] red dashed line represents the electrical conductivity of adularia single crystal ($Or_{84}Ab_{16}$) at atmospheric pressure from Maury;[23] green dashed line represents the electrical conductivity of alkali feldspar ($Or_{61}Ab_{34}An_5$) at atmospheric pressure from Mizutani and Kanamori.[22]

The logarithm of the electrical conductivity at each pressure and orientation varies linearly with the reciprocal of temperature, indicating that our samples have only a single dominant conduction mechanism. The activation volume (ΔV) is established to be directly related to the conduction mechanism.[52–57] The ionic conduction mechanism of minerals with silicate and carbonate frameworks is characterized by a positive value of the order from several to several tens of cm^3/mole.[58,59] The 2.51-cm^3/mole activation volume calculated here suggests that the dominant conduction mechanism of K-feldspar at high temperatures and high pressures involves interstitial potassium ions, which agrees with all of the previous results for tectosilicate minerals.[28–34] The interstitial ionic potassium is formed according to the point defect reaction as follows:[60]

$$K_{\mathrm{Al}}^{\times} + V_{\mathrm{i}} \rightleftharpoons K_{\mathrm{i}}^{\bullet} + V'_{\mathrm{Al}}, \tag{10}$$

where $K_{\mathrm{A1}}^{\times}$ and V'_{A1} represent the potassium ion and a vacancy at the A1 site of the normal lattice, respectively, and $K_{\mathrm{i}}^{\bullet}$ and V_{i} refer to the potassium ion and a vacancy in the interstitial site, respectively. The dominant charge carrier of K-feldspar is the interstitial ionic potassium ($K_{\mathrm{i}}^{\bullet}$), which contributes to conduction by hopping between the A1 site of the normal lattice and the adjacent interstitial sites along thermally activated electric fields under certain conditions of temperature, pressure, and crystallographic axis direction, thus producing a vacancy by Frenkel pair formation.

4.3. Calculated *K* diffusion coefficient

Electrical conductivity originates from the diffusion of a dominant charge-carrying species under a designated AC electric field. The correlation between electrical conductivity and isotope diffusion coefficient has been widely examined for many silicate minerals in order to link measured conductivities, the conduction mechanism, and diffusion data for charge carriers (e.g., ions, small polarons, protons etc.).[61–68] The K-feldspar studied here had only potassium ions at the interstitial sites verified to play an important role in bulk conductivity, and their diffusion coefficient can be obtained from the Nernst–Einstein equation:[69]

$$\sigma = fDcq^2/kT, \tag{11}$$

where σ is the electrical conductivity of K-feldspar (S/m), D is the diffusion coefficient of the charge carrier (cm^2/s), c is the number of charge carriers per volume unit, expressed as $n = N_{\mathrm{A}}\rho L/M$ (1/m^3) (where N_{A} is the Avogadro's number, ρ is the density of K-feldspars, M is the molecular weight, and L is the number of potassium atoms per molecule), q is the electrical charge quantity of the charged species (Coulomb), f is the dimensionless correction correlation factor (related to the Haven ratio, H_{r}), which is usually between 0.5 and 1.0, k is the Boltzmann constant (in units J/K), and T is the absolute temperature (in unit K). The value of H_{r} depends on the diffusion mechanism: the interstitial mechanism for $f = 1.0$ and other mechanisms for $f < 1.0$ (e.g., the vacancy or sublattice interstitial mechanisms).[70] Here, $f = 1$ is assumed for K-feldspar, and we can describe the transport of potassium ions by a process other than volume diffusion by Fick's law. On the assumption that only potassium ions are involved in the transport process, equation (11) can be used to calculate their diffusion coefficient from the electrical conductivity data of anisotropic K-feldspar at 2.0 GPa; the results are illustrated in Fig. 11 together with those from the previous studies.

Figure 11 shows that the calculated K diffusion coefficients along the different crystallographic axes, plotted in the Arrhenius diagram, display linear relationships and fall within a range of 10^{-12} m^2/s–10^{-9} m^2/s at 2.0 GPa over a wide temperature range of 873 K–1223 K. The degree of anisotropy of the diffusion coefficient (the ratio of the maximum along

the $\perp[001]$ axis to the minimum in the $\perp[100]$ direction, D_{max}/D_{min}) for K-feldspar is ~ 4, which is somewhat consistent with the results of recent diffusion experiments by Wilangowski *et al.*,[66] confirming that the radioisotope ^{22}Na may be used as a tracer that the diffusion coefficient of single-crystal VF feldspar along the $\perp[001]$ orientation is larger than in the $\perp[101]$ direction, although the difference is only 20%.

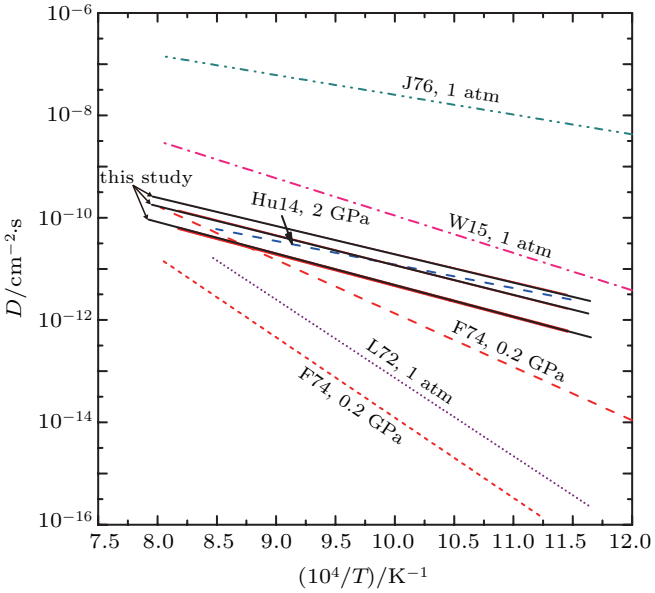


Fig. 11. (color online) Calculated diffusion coefficients of dry K-feldspar single crystal by using the Nernst–Einstein equation at 2.0 GPa, and their comparison with previous studies. Black solid lines represent the results of this work; pink dotted line represents the self-diffusion coefficient of sodium in natural single-crystal alkali sanidine with a chemical composition of $X_K = 0.85$ at room pressure from Wilangowski *et al.*;[66] blue dashed line represents the calculated average diffusion coefficient of potassium ions in polycrystalline K-feldspar aggregate along different orientations at 2.0 GPa from Hu *et al.*;[30] green dashed line represents the potassium diffusion coefficient of orthoclase glass at room pressure from Jambon and Carron;[73] red dotteded and dash lines represent the self-diffusion coefficients of potassium and sodium ions for the natural orthoclase ($X_K = 0.94$) at 0.2 GPa from Foland,[72] respectively; purple dotted line represents the *K* self-diffusion coefficient for pure microcline perthite ($X_K = 0.888$) at room pressure from Lin and Yund.[71]

In light of this new result for the influence of crystallographic orientation on the diffusion coefficient of single-crystal K-feldspar, we compare five previous results obtained under different conditions. Lin and Yund[71] found the potassium self-diffusion coefficient for pure microcline perthite with a chemical composition of $X_K = 0.888$ by using a ^{40}K tracer at 873 K–1073 K and ambient pressure. Foland[72] measured diffusivities of sodium and potassium ions for natural orthoclase with a chemical composition of $X_K = 0.94$ via a hydrothermal bulk-exchange experiment at 0.2 GPa and 773 K–1073 K. The diffusion coefficients obtained here are clearly higher than those for K self-diffusion given by Lin and Yund[71] and Foland,[72] but our results are very close to the self-diffusion coefficients of potassium and sodium ions reported by Foland[72] at high temperature. The activation energy calculated in this work (1.04 eV) is lower than the 3.43 eV obtained by Lin and Yund[71] and the 2.30 eV–2.96 eV reported by Foland.[72] Jambon and Carron[73] measured the potassium diffusion coefficient in orthoclase glass by using the technique of active salt deposits at 573 K–1273 K and atmospheric pressure; its result was abnormally higher than all of other reported results as shown in Fig. 9. Compared with our obtained experimental result, previous data for the K diffusion coefficient show a large discrepancy,[71–73] which might be due to differences in chemical composition, measurement condition, or experimental technique. Hu *et al.*[30] measured the electrical conductivity of dry, pure, polycrystalline sintered K-feldspar by AC impedance spectroscopy, and calculated an average diffusion coefficient of potassium ions along different orientations at 1.0 GPa–3.0 GPa and 873 K–1273 K. Wilangowski *et al.*[66] reported the self-diffusion coefficient of sodium at 777 K–1173 K in natural single-crystal alkali sanidine ($X_K = 0.85$) from Volkesfeld (Eifel, Germany) by self-diffusion experiments and theoretical Monte Carlo simulations, and found two crucial factors — alkali compositions (X_K) and jump frequencies —that can cause significant discrepancies in the reported diffusion coefficients. The results for polycrystalline K-feldspar aggregate and single-crystal sanidine[30,66] show a good consistency with our anisotropic diffusion coefficients obtained at 1.0 GPa–3.0 GPa and 873 K–1223 K. The 1.04 eV activation energy obtained here for K-feldspar is also very close to other values for K-rich feldspars. For example, the electrical conductivity was measured by Hu *et al.* to be 0.98 eV[30] and it was 1.30 eV from the Monte Carlo simulations by Wilangowski *et al.*[66]

5. Summary

In summary, in the present study, strong anisotropies along the three main orientations in both the electrical conductivity and the potassium diffusion coefficient of K-feldspar are revealed by using the electrochemical impedance spectra at conditions of high temperature and high pressure, with anisotropic ratios ($\sigma_{max}/\sigma_{min}$ and D_{max}/D_{min}) of approximately 3–4. All of these results suggest that the interstitial ionic potassium as one of potential conduction mechanisms, plays an important role in the electrical transport and diffusion migration of charge carriers in each crystallographic direction. As a matter of fact, the actual anisotropic contributions from electrical conductivities and diffusion coefficients of mineral and rock at high pressure depend on not only their own magnitude but also the volume percentage of sample in the earth's interior.[74] It is well known that feldspar with a largest volume percentage is of a 60% main rock-forming mineral in the deep earth's crust. So, in the present study, our observable strong anisotropy for feldspar single crystal in electrical conductivity at high temperature and high pressure maybe has an

extremely large contribution to reasonably explain the anomalously high conductivity zone under the stable mid-lower continental crust.

Acknowledgement

We appreciate Dr. Aaron Stallard of Stallard Scientific Editing Company for polishing the English language of the manuscript.

References

[1] Huang X G, Xu Y S and Karato S I 2005 *Nature* **434** 746
[2] Wang D J, Mookherjee M, Xu Y S and Karato S I 2006 *Nature* **443** 977
[3] Huang X G, Bai W M and Zhou W G 2008 *Chin. J. High Press. Phys.* **22** 237 (in Chinese)
[4] Huang X G, Huang X G and Bai W M 2012 *Chin. J. Geophys.* **55** 3144
[5] Dai L D, Hu H Y, Li H P, Jiang J J and Hui K S 2014 *Am. Mineral.* **99** 1420
[6] Huang X G, Wang X X, Chen Z A and Bai W M 2017 *Sci. Sin. Terrae* **47** 518
[7] Liu X, Dai L D, Deng L W, Fan D W, Liu Q, Ni H W, Sun Q, Wu X, Yang X Z, Zhai S M, Zhang B H, Zhang L and Li H P 2017 *Chin. J. High Press. Phys.* **31** 657 (in Chinese)
[8] Mareschal M, Kellett R L, Kurtz R D, Ludden J A, Ji S and Bailey R C 1995 *Nature* **375** 134
[9] Evans R L, Tarits P, Chave A D, White A, Heinson G, Filloux J H, Toh H, Seama N, Utada H, Brook J R and Unsworth M J 1999 *Science* **286** 752
[10] Liu J L, Bai W M, Kong X R and Zhu M X 1999 *Chin. J. Geophys.* **44** 528
[11] Evans R L, Hirth G, Baba K, Forsyth D, Chave A and Mackie R 2005 *Nature* **437** 249
[12] Dai L D and Karato S I 2014 *Earth Planet. Sci. Lett.* **408** 79
[13] Novella D, Jacobsen B, Weber P K, Tyburczy J A, Ryerson F J and Du Frane W L 2017 *Sci. Rep.* **7** 5344
[14] Tolland H G 1973 *Nature* **241** 35
[15] Huebner J S and Voigt D E 1988 *Am. Mineral.* **73** 1235
[16] Bagdassarov N S and Delépine N 2004 *J. Phys. Chem. Solids* **65** 1517
[17] Dai L D and Karato S I 2009 *Proc. Jpn. Acad. Ser. B* **85** 466
[18] Yang X Z, Keppler H, McCammon C and Ni H W 2012 *Contrib. Mineral. Petrol.* **163** 33
[19] Li Y, Jiang H T and Yang X Z 2017 *Geochim. Cosmochim. Ac.* **217** 16
[20] Noritomi K 1955 *Sci. Rep. Tohoku. Univ. Ser.* **56** 119
[21] Khitarov N and Slutskiy A 1965 *Geochem. Int.* **2** 1034
[22] Mizutani H and Kanamori H 1967 *J. Phys. Earth* **15** 25
[23] Maury R 1968 *Bulletin de la Societe Francaise de Mineralogie et Cristallographie* **91** 355
[24] Piwinskii A J and Duba A G 1974 *Geophys. Res. Lett.* **1** 209
[25] Piwinskii A J, Duba A G and Ho P 1977 *Can. Mineral.* **15** 196
[26] Guseinov A A and Gargatsev I O 2002 *Izv-Phys. Solid Earth* **38** 520
[27] Bakhterev V V 2008 *Doklady Earth Sci.* **420** 554
[28] Hu H Y, Li H P, Dai L D, Shan S M and Zhu C M 2011 *Am. Mineral.* **96** 1821
[29] Hu H Y, Li H P, Dai L D, Shan S M and Zhu C M 2013 *Phys. Chem. Minerals* **40** 51
[30] Hu H Y, Dai L D, Li H P, Jiang J J and Hui K S 2014 *Mineral. Petrol.* **108** 609
[31] Hu H Y, Dai L D, Li H P, Hui K S and Li J 2015 *Solid State Ionics* **276** 136
[32] Ni H W, Keppler H, Manthilake M and Katsura T 2011 *Contrib. Mineral. Petrol.* **162** 501
[33] Wang D J, Yu Y J and Zhou Y S 2014 *High Pressure Res.* **34** 297
[34] El Maanaoui H, Wilangowski F, Maheshwari A, Wiemhöfer H D, Abart R and Stolwijk N A 2016 *Phys. Chem. Minerals* **43** 327
[35] Liu X, Hu Z Y and Deng L W 2010 *Acta Petrol. Sin.* **26** 3641
[36] Paterson M S 1982 *Bull. Mineral.* **105** 20
[37] Mosenfelder J, Rossman G and Johnson E 2015 *Am. Mineral.* **100** 1209
[38] Hui K S, Zhang H, Li H P, Dai L D, Hu H Y, Jiang J J and Sun W Q 2015 *Solid Earth* **6** 1037
[39] Sun W Q, Dai L D, Li H P, Hu H Y, Wu L and Jiang J J 2017 *Am. Mineral.* **102**, in press
[40] Shan S M, Wang R P, Guo J and Li H P 2007 *Chin. J. High Press. Phys.* **21** 367
[41] Xu J A, Zhang Y M, Hou W, Xu H S, Guo J, Wang Z M, Zhao H, Wang R, Huang E and Xie H S 1994 *High Temp. High Press.* **26** 375
[42] Roberts J J and Tyburczy J A 1991 *J. Geophys. Res.* **96** 16205
[43] Roberts J J and Tyburczy J A 1993 *Phys. Chem. Minerals* **20** 19
[44] Roberts J J and Duba A G 1995 *Geophys. Res. Lett.* **22** 453
[45] Hu H Y, Dai L D, Li H P, Hui K S and Sun W Q 2017 *J. Geophys. Res.* **122** 2751
[46] Jones A G, Palmer D, Islam M S and Mortimer M 2004 *Phys. Chem. Minerals* **31** 313
[47] Karato S I and Dai L D 2009 *Phys. Earth Planet. Inter.* **174** 19
[48] Hirsch L M, Shankland T J and Duba A G 1993 *Geophys. J. Int.* **114** 36
[49] Dai L D and Karato S I 2014 *Phys. Earth Planet. Inter.* **237** 73
[50] Romano C, Poe B T, Kreidie N and McCammon C A 2006 *Am. Mineral.* **91** 1371
[51] Dai L D, Li H P, Hu H Y, Shan S M, Jiang J J and Hui K S 2012 *Contrib. Mineral. Petrol.* **163** 689
[52] Xu Y S, Shankland T J and Duba A G 2000 *Phys. Earth Planet. Inter.* **118** 149
[53] Dai L D and Karato S I 2009 *Phys. Earth Planet. Inter.* **176** 83
[54] Ono S and Mibe K 2013 *Eur. J. Mineral.* **25** 11
[55] Dai L D and Karato S I 2014 *Phys. Earth Planet. Inter.* **232** 51
[56] Ono S and Mibe K 2015 *Phys. Chem. Minerals* **42** 773
[57] Dai L D, Hu H Y, Li H P, Wu L, Hui K S, Jiang J J and Sun W Q 2016 *Geochem. Geophys. Geosyst.* **17** 2394
[58] Samara G A 1984 *Solid State Phys.* **38** 1
[59] Mibe K and Ono S 2011 *Physica B* **406** 2018
[60] Behrens H, Johannes W and Schmalzried H 1990 *Phys. Chem. Minerals* **17** 62
[61] Dai L D and Karato S I 2009 *Phys. Earth Planet. Sci. Lett.* **287** 277
[62] Du Frane W L and Tyburczy J A 2012 *Geochem. Geophys. Geosyst.* **13** Q03004
[63] Yang X Z 2012 *Earth Planet. Sci. Lett.* **317** 241
[64] Dai L D and Karato S I 2014 *Phys. Earth Planet. Inter.* **232** 57
[65] Karato S I 2015 *Phys. Earth Planet. Inter.* **248** 94
[66] Wilangowski F, Abart R, Divinski S V and Stolwijk N A 2015 *Defect and Diffusion Forum* (Zurich: Trans Tech Publications Inc.) pp. 79–84
[67] Jones A G 2016 *Phys. Chem. Minerals* **43** 237
[68] Zhao C C and Yoshino T 2016 *Earth Planet. Sci. Lett.* **447** 1
[69] Karato S I 1990 *Nature* **347** 272
[70] Isard J O 1999 *J. Non-cryst. Solids* **246** 16
[71] Lin T H and Yund R A 1972 *Contrib. Mineral. Petrol.* **34** 177
[72] Foland K A 1974 *Geochemical Transport and Kinetics* (Washington: Carnegie Institute of Washington) pp. 77–98
[73] Jambon A and Carron J 1976 *Geochim. Cosmochim. Ac.* **40** 897
[74] Dai L D, Li H P, Hu H Y, Jiang J J, Hui K S and Shan S M 2013 *Tectonophysics* **608** 1086